

See discussions, stats, and author profiles for this publication at: <https://www.researchgate.net/publication/221794166>

Model Shape Transitions of Micelles: Spheres to Cylinders and Disks

ARTICLE *in* LANGMUIR · FEBRUARY 2012

Impact Factor: 4.46 · DOI: 10.1021/la204132c · Source: PubMed

CITATIONS

14

READS

56

3 AUTHORS, INCLUDING:



[Asfaw Gezae](#)

Stellenbosch University

9 PUBLICATIONS 36 CITATIONS

[SEE PROFILE](#)



[Josep Bonet Avalos](#)

Universitat Rovira i Virgili

70 PUBLICATIONS 1,208 CITATIONS

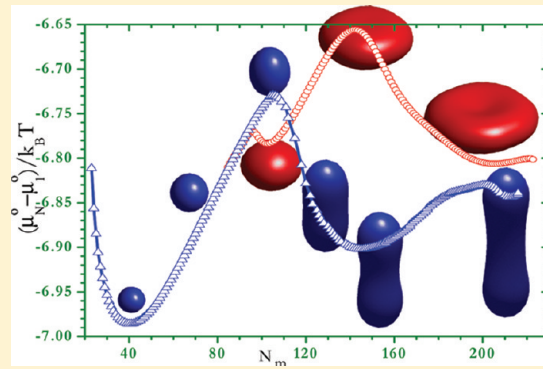
[SEE PROFILE](#)

Model Shape Transitions of Micelles: Spheres to Cylinders and Disks

¹ Asfaw Gezae Daful, Josep Bonet Avalos, and Allan D. Mackie*

³ Departament d'Enginyeria Química, ETSEQ, Universitat Rovira i Virgili, Av. dels Països Catalans 26, 43007 Tarragona, Spain

ABSTRACT: We present a microscopic analysis of shape transitions of micelles of model linear nonionic surfactants. In particular, symmetric H_4T_4 and asymmetric H_3T_6 surfactants have been chosen for the study. In a previous work, it has been observed that symmetric surfactants have a strong tendency to prefer spherical micelles over a wide range of chemical potentials, while asymmetric surfactants undergo shape transitions between the spherical micelle at low concentration to other forms, mainly finite cylindrical micelles. This study combines the application of a two-dimensional single-chain mean-field theory (SCMFT) with Monte Carlo (MC) simulations of exactly the same systems. On the one hand, the characteristics of the SCMFT make this method suitable for free energy calculations, especially for small surfactants, due to the incorporation of relevant microscopic details in the model. On the other hand, MC simulations permit us to obtain a complete picture of the statistical mechanical problem, for the purpose of validation of the mean-field calculations. Our results reveal that the spherical shape for the symmetric surfactant is stable over a large range of surfactant concentrations. However, the asymmetric surfactant undergoes a complex shape transition that we have followed by calculating the standard chemical potential as a function of the aggregation number. The results indicate that the system forms prolate spheroids prior to developing short capped cylinders that gradually grow in length, with some oscillations in the energy of formation. The most important result of our work is the evidence of a bifurcation where, together with the elongated objects, the system can develop oblate aggregates and finally a shape like a red blood cell.



1. INTRODUCTION

Above the critical micellar concentration, amphiphilic molecules in aqueous solutions spontaneously self-assemble into aggregates or microstructures known as micelles. Driven by the hydrophobicity of the tails and the hydrophilic nature of the head groups of the surfactant, they are capable of spontaneously self-assembling into aggregates of different geometric shapes such as spheres, ellipsoids, cylinders, disks, bilayers, vesicles, etc. Normally, at low concentrations close to the so-called critical micelle concentration (cmc), small spherical micelles are formed; however, changes in the solution conditions, such as surfactant concentration, temperature, and other physicochemical parameters, can cause changes in the micellar morphology,^{1–17} which can be termed as shape transitions.

This rich diversity of micellar morphologies plays an increasingly important role in many biological and industrial processes, such as in drug loading and delivery, catalysis, cosmetics, and separation processes in engineering and environmental science and technology. Interestingly, all these applications depend on the capability to tune and control the shape and size of the aggregates that surfactants form in solution. The size, shape, and structure of micelles are thus important characteristics in determining their main properties and areas of application.^{1–5,18} As an example, the shape and size of micelles can strongly influence the viscosity^{2,19} and other rheological features of the solution.

The question of the shape of the micelle has received considerable attention from several investigators. For instance, experimentally Debye et al.²⁰ and Eriksson²¹ showed that the micelles can undergo a transition from spherical to rodlike aggregates upon increasing surfactant concentration above the cmc. This idea has been supported by many other experimental works using, for example, NMR,^{22–24} viscosity,^{25,26} turbidity,^{27–29} dynamic light scattering,^{29,30} static light scattering,^{31–34} cryo-TEM,^{35–38} TEM,^{27,39,40} and SANS.^{41–45} Recent studies have expanded the variety of micellar shapes to unconventional forms that include disks,^{46–48} toroids,^{47,49,50} tubes,⁵¹ and helices,⁵² among others.

From a modeling perspective, an empirical relation for micellar structure, based upon the geometry of various micellar shapes and the space occupied by the hydrophilic and hydrophobic groups of the surfactant molecules, was developed by Israelachvili.¹ May and Ben-Shaul⁵³ modeled the sphere to cylinder transition using a spherocylinder model, where they assumed that the packing free energy of the micelle is a sum of contributions from amphiphilic molecules packed in the cylindrical body and the two hemispherical end-caps. Zaid et al.¹¹ used a spherocylindrical model, from single-chain mean-field theory (SCMFT), assuming a linear combination of the

Received: October 21, 2011

Revised: January 10, 2012

73 standard chemical potentials of independent spherical and
 74 infinite cylindrical micelles. They found that the symmetric
 75 surfactant, H_4T_4 , favors the formation of spherical micelles,
 76 while the asymmetric H_3T_6 amphiphile prefers to form
 77 cylindrical micelles at higher amphiphile concentrations,
 78 where the term H_xT_y refers to a surfactant with x head and y
 79 tail segments, respectively. These authors characterize a second
 80 cmc to define the transition from spheres to cylinders. Jódar-
 81 Reyes et al.,⁹ in turn, used a 2D self-consistent field theory
 82 (SCF) to analyze the micellar shape transition in nonionic
 83 surfactants of the type C_nE_m . The grand potential⁹ and free
 84 energy⁵³ of the cylindrical micelle were reported to have an
 85 oscillatory behavior with an amplitude that decays with the
 86 length of the body of the cylinder. According to these models
 87 for micellar growth,^{9,11,53} the sphere to rod transition should be
 88 regarded as a continuous crossover process, with the average
 89 micellar size increasing as a function of the surfactant
 90 concentration and, ultimately, of the chemical potential.

91 Monte Carlo simulations^{54–59} have also been used to study
 92 micellar shapes and sizes. Xuehao et al.⁵⁴ applied the Monte
 93 Carlo method to study the self-assembly of amphiphilic diblock
 94 copolymers in a selective solvent. They illustrated the
 95 dependence of the aggregate morphologies of their diblock
 96 copolymers in solution on the length of the corona-forming
 97 segments. They found that on decreasing the corona-forming
 98 segments, a transition from spherical micelles to rodlike
 99 aggregates occurs. Monte Carlo simulations by Termonia⁵⁸
 100 show the effect of the length, x , of the hydrophilic block on the
 101 final aggregate morphology of an amphiphile H_xT_y in pure
 102 water. They show the formation of spherical micelles for
 103 surfactants with $x \geq y$ and cylindrical micelles for surfactants
 104 with $x < y$.

105 Molecular dynamic simulations have been carried out in
 106 order to address the structural properties of micelles.^{60,61}
 107 Marrink et al.⁶⁰ showed the spontaneous aggregation of the
 108 dodecylphosphocholine surfactant into spherical micelles at low
 109 concentrations, while stable wormlike micelles appear at higher
 110 concentrations. Fujiwara et al.⁶¹ studied how the micellar shape
 111 changes depending on the hydrophilicity and hydrophobicity of
 112 the amphiphilic molecule H_1T_2 . They observe three kinds of
 113 isolated micelles, i.e., discoidal, cylindrical, and spherical
 114 micelles, by varying the intensity of the hydrophilicity and
 115 hydrophobicity.

116 The variety of micellar shapes to other forms has also been
 117 observed in simulations. These include disks,^{46–48,62,63}
 118 toroids,^{47,49,50,64} tubes,⁵¹ and even helices.⁵² Nevertheless, a
 119 comprehensive microscopic understanding of the concentra-
 120 tion-induced shape transition is still missing, in particular, the
 121 relationship between surfactant architecture and the hydro-
 122 phobic–hydrophilic interactions and the dependence of the
 123 shape on concentration and temperature.

124 The main purpose of this work is to present a detailed
 125 exploration of the process of shape transition in nonionic
 126 surfactant aggregates with varying surfactant concentration,
 127 paying attention to the different shapes that occur in the
 128 process and their free energy of formation. The analysis is
 129 carried out using one and two-dimensional SCMFT together
 130 with Monte Carlo simulations. In both cases the surfactants are
 131 defined on a lattice and the same H_xT_y surfactant model is used.
 132 With respect to previous works, SCMFT provides a suitable
 133 framework to study this kind of system, due to mainly two
 134 aspects. On the one hand, SCMFT yields accurate estimates of
 135 the energy of formation of the different aggregates that appear

in the system. In the present work, we have extended the 136 analysis of our previous study¹¹ to two dimensions, to relax the 137 description of the aggregate as a combination of shapes arising 138 from one-dimensional calculations. Therefore, shapes other 139 than spherocylinders can be directly described. Moreover, 140 unlike other self-consistent field calculations based on Gaussian 141 statistics, the self-avoidance of the conformations permits a 142 direct comparison with results obtained from Monte Carlo 143 simulations. On the other hand, extensive Monte Carlo 144 simulations allow us to elucidate and confirm the shapes that 145 the SCMFT produce. Furthermore, the Monte Carlo results 146 provide additional insight into the role of the shape 147 fluctuations, which complement the conclusions drawn from 148 the 2D-SCMFT. This parallel view of the problem permits us 149 to speculate on likely energy landscapes underlying the shape 150 behavior of these types of surfactants, in an area where precise 151 and conclusive experimental data are either scarce or 152 nonexistent. As compared to previous self-consistent field 153 calculations,^{9,53} our results also reproduce the oscillatory 154 behavior in the free energy of formation for moderately short 155 cylinders, but we explore in detail the region of the transition 156 itself, where we have found the most interesting result. 157 Effectively, our analysis reveals the existence of a bifurcation 158 leading either to finite cylinders or disks. Each branch has its 159 own dependence of the free energy on the aggregation number, 160 but they have a tendency to merge at large aggregation 161 numbers. Indeed, the two branches are different paths toward 162 the same infinite cylinder and therefore should approach the 163 same free energy.

Monte Carlo simulations clearly show the existence of a few, 165 energetically less-favorable, disks coexisting with short capped 166 cylinders, in perfect agreement with the interpretation of the 167 energetic results obtained from the SCMFT.

The paper is organized as follows. In section 2, the lattice 169 model is described. In section 3 we introduce the two- 170 dimensional (SCMFT). We continue with section 4, where the 171 details of the simulation are given, followed by section 5 172 devoted to the analysis of the results. Finally, the paper finishes 173 with section 6, where the main conclusions are reviewed.

2. THE MODEL

In this section we describe the lattice model used in the present 175 work for nonionic surfactant systems, originally proposed by 176 Larson.⁶⁵ We considered an $L \times L \times L$ cubic lattice completely 177 occupied by solvent and surfactant molecules. We take the 178 lattice spacing as being the unit of length and then L stands for 179 the number of lattice sites per dimension. In this model, each 180 solvent molecule (properties of the solvent will be indexed with 181 S), is a single unit occupying one lattice site. The linear 182 amphiphilic molecules, H_xT_y occupy a set of connected sites, 183 where H and T are the hydrophilic head and hydrophobic tail 184 units, respectively, while the subscripts x and y denote the 185 number of segments in the headgroup and tail group, 186 correspondingly. A particle occupying a given site interacts 187 with its $z = 26$ nearest or diagonally nearest neighbors, both 188 indistinctly referred to as nearest neighbors from here on. In 189 this work, the solvent molecules are assumed to be identical to 190 the head groups as far as interaction energy is concerned. Thus, 191 a site occupied either by a solvent or by a head segment 192 interacts with a similar nearest neighboring site through an 193 interaction energy ϵ_{HH} . The tail–tail and head–tail interaction 194 energies are denoted by ϵ_{TT} and ϵ_{HT} , respectively. For a 195

196 completely occupied lattice, the equation for changes in the
197 total energy of the system depends upon one single parameter

$$\varepsilon \equiv \varepsilon_{HT} - \frac{1}{2}(\varepsilon_{HH} + \varepsilon_{TT}) \quad (1)$$

198 due to the conservation of the number of contacts.⁶⁶
199 Furthermore, we define the dimensionless temperature, $T^* =$
200 $k_B T / \varepsilon$. In this work ε_{TT} is arbitrarily set to -2 (resulting in
201 attractive interactions for nearest-neighbor tail-tail contact),
202 while ε_{HH} and ε_{HT} are arbitrarily set to zero^{11,67,68} since only
203 the value of ε is relevant as a thermodynamic parameter.

3. SINGLE CHAIN MEAN FIELD THEORY

204 The single-chain mean-field theory (SCMFT) is a mean-field
205 approach based on the generation of single-chain config-
206 urations, from a microscopically detailed model for the chain in
207 a mean-field. It was originally developed to study the molecular
208 organization of amphiphilic tails in dry core aggregates and later
209 generalized to include solvent molecules.^{53,69,70} The imple-
210 mentation of the theory for surfactant self-assembly without the
211 dry core restriction was presented for lattice chains by Mackie
212 et al.⁶⁷

213 In relation with previous works, in this paper the mean-field
214 equations will be explicitly formulated for two-dimensional
215 fields. In particular, the field is divided into Z_l layers along the
216 z -axis and N_c concentric shells of radii r in the xy plane, since
217 only axisymmetric geometries will be considered. The excluded
218 volume interactions in the chain conformations are explicitly
219 taken into account, while those through the mean-field are
220 introduced from the constraint of single occupancy, i.e., by the
221 fact that the sum of average volume fractions of the head, tail
222 and the solvent monomers is unity,

$$\langle \phi_S(r, z) \rangle + \langle \phi_T(r, z) \rangle + \langle \phi_H(r, z) \rangle = 1 \quad (2)$$

223 where $\phi_i(r, z)$, is the volume fraction of species i in layer z and
224 shell r .

225 The average chain potential energy is a sum of intramolecular
226 and intermolecular interactions. The intramolecular energy per
227 chain in the aggregate is exactly calculated from the positions of
228 all the monomers in each chain conformation, which is defined
229 by the number of monomer-monomer tail contacts n_{TT}^{intra} , for
230 the case where only $\varepsilon_{TT} \neq 0$ is considered. Therefore, its
231 average reads

$$\langle E_{intra} \rangle = \varepsilon_{TT} \sum_{\alpha} P(\alpha) n_{TT}^{intra}(\alpha) \quad (3)$$

232 where α and $P(\alpha)$ are, respectively, a given conformation and
233 its probability. The intermolecular chain-chain interaction
234 term is described as the interaction between the given chain
235 and the mean-field in its surroundings

$$\langle E_{inter} \rangle = \frac{\varepsilon_{TT}}{2} \sum_z \sum_r \langle n_{n,T}(r, z) \rangle \langle \phi_T(r, z) \rangle \quad (4)$$

236 where $\langle n_{n,T}(r, z) \rangle$ is the average number of available nearest
237 neighbor sites in the particular r, z layer. In our case, since only
238 T segments have potential interaction, only this species is
239 considered.

The entropy of the system contains two contributions,
240 namely, the entropy of the amphiphiles and that of the solvent
241 molecules
242

$$\frac{S}{k_B} = -N \sum_{\alpha} P(\alpha) \ln P(\alpha) - \sum_z \sum_r n_S(r, z) \ln \phi_S(r, z) \quad (5)$$

where n_S is the number of solvent sites in layer z and shell r and
243 N is the number of chains in the system.
244

The configurational free energy of the system is then given
245 by
246

$$\frac{F}{k_B T} = \beta N [\langle E_{inter} \rangle + \langle E_{intra} \rangle] - \frac{S}{k_B} \quad (6)$$

The probability distribution function, $P(\alpha)$, and solvent
247 density profile, $\phi_S(r, z)$, are found from a functional
248 minimization of the free energy (eq 6) subject to the packing
249 constraints (eq 2). This functional minimization is done by
250 introducing the set of Lagrange multipliers, $\pi(r, z)$. The
251 probability distribution function, $P(\alpha)$, is obtained as
252

$$P(\alpha) = \frac{\exp\{-\mathcal{H}[\alpha]\}}{\sum_{\alpha} \exp\{-\mathcal{H}[\alpha]\}} \quad (7)$$

where $\mathcal{H}[\alpha]$ is the mean-field Hamiltonian
253

$$\begin{aligned} \mathcal{H}[\alpha] = & \sum_z \sum_r \pi(r, z) [n_H(\alpha, r, z) + n_T(\alpha, r, z)] \\ & + \chi_{TT} n_{TT}^{intra}(\alpha) + \frac{\chi_{TT}}{2} \sum_z \sum_r \frac{N-1}{V(r, z)} \\ & [n_{n,T}(\alpha, r, z) \langle n_T(r, z) \rangle + \langle n_{n,T}(r, z) \rangle n_T \\ & (\alpha, r, z)] \end{aligned} \quad (8)$$

We define the dimensionless interaction parameter $\chi_{TT} = \beta \varepsilon_{TT}$
254 = $1/T^*$, where $\beta = 1/k_B T$.
255

The solvent density profile is given by
256

$$\varphi_S(r, z) = \exp[-\pi(r, z)] \quad (9)$$

The value of the Lagrange multipliers has to be found self-
257 consistently from the equation of the constraint itself (eq 2),
258 which implicitly depends upon $\pi(r, z)$ through the expressions
259 of the probability distribution as well as the solvent density
260 profile, i.e.
261

$$\begin{aligned} & \sum_{\alpha} \left\{ P(\alpha) \frac{N-1}{V(r, z)} [n_H(\alpha, r, z) + n_T(\alpha, r, z)] \right\} \\ & + e^{-\pi(r, z)} = 1 \quad \forall_{r,z} \end{aligned} \quad (10)$$

which is a set of nonlinear self-consistent equations that can be
262 solved by standard numerical methods.
263

The difference in standard chemical potential between free
264 chains, μ_1^o , and micelles of size N , μ_N^o , is calculated by way of⁷¹
265

$$\exp\left(-\frac{\mu_N^o - \mu_1^o}{k_B T}\right) \approx \frac{V}{N} \frac{\sum_{\alpha} \exp\left(-\frac{\mathcal{H}_N[\alpha]}{k_B T}\right) / W(\alpha)}{\sum_{\alpha} \exp\left(-\frac{\mathcal{H}_1[\alpha]}{k_B T}\right) / W(\alpha)} \quad (11)$$

where V is the volume of the simulation box (L^3), and $W(\alpha)$ is
266 the statistical weight of the chain conformation in the sampling
267

used to generate it. In particular, the exponent $(\mu_N^0 - \mu_1^0)/k_B T$ represents the difference in free energy cost of introducing one surfactant in the simulation box, containing the micelle in its center, as compared to the reference state. Such a reference state has been taken as being the free energy of a system of one surfactant with the first monomer constrained to the center of the same box. Notice that in the latter, there is an entropic contribution only due to the conformational changes of the chain. Moreover, the superscript 0 indicates that there is a translational degree of freedom frozen in both the actual and the reference systems during the calculation (see ref 71 for a complete derivation of the right-hand side of equation eq 11).

4. METHODOLOGY

4.1. The SCMFT. The sampling of the one-chain configurational space is done by generating chain conformations in a cubic box of volume V . The solution of the mean-field equations considers the presence of N amphiphilic molecules at a temperature T . The amphiphile configurations are obtained using the Rosenbluth and Rosenbluth chain growth self-avoiding random walk algorithm,⁷² and periodic boundary conditions are applied in all directions. It is important to note at this point that the set of generated configurations, α , also include the random sampling of the positions of the first segment of the chain inside the box.

Spherical micelles and infinite cylindrical micelles have in common that the mean-field is a function of one single variable, the distance to the center of the sphere or to the axis of the cylinder, respectively.¹¹ It is evident that the choice, a priori, of these geometries constrains the mean field to be of this form. Therefore, no shape transition can be studied within a 1D geometry. However, these calculations are relevant limiting cases that will serve as a reference for the more general 2D simulations.

To obtain these 1D solutions of the mean field equations, 10^6 chain configurations were randomly generated in a field divided into one-dimensional spherical or cylindrical shells with a width of one lattice spacing, in a simulation box of volume 19^3 . When solving the field, we verified that the same solution was obtained when using 10^7 configurations, for the same box size.

In the case of the 2D discretization of space, we have assumed that the micelles are bodies of revolution, the mean-field depending only on the position on the revolution axis and the distance to it. Thus, the simulation box is divided into Z_l slices with a width of one lattice unit as described in section 3. The shell volume, $V(r,z)$, is defined by counting the number of sites included in each circular shell of a given layer. A site is considered to be included in a shell if its center falls within the shell as defined in continuous space. To include the corners of the simulation box, the last shell has a different geometry and occupies the volume from the surface of the previous cylindrical shell to the borders of the box. In that region, it is assumed that the field is constant and should describe the bulk system. We have proceeded in an analogous fashion for the 1D system.

For the 2D case, the systems are cubic boxes of 25^3 , 27^3 , and 35^3 lattice sites, with 2×10^6 , 4×10^6 , and 6×10^6 configurations generated, respectively. The self-consistent solution of the mean-field equations yields the Lagrange multipliers, $\pi(r,z)$, which are required to obtain the physical probability distribution function for a given conformation α , namely, $P(\alpha)$. Once the probability distribution is known, all physical averages then follow, $\langle n_T(r,z) \rangle$ and $\langle n_H(r,z) \rangle$, and the problem is fully determined. Typical times for convergence of

these equations for the 2D case go from minutes to hours on a standard serial workstation, depending on the box size and the number of configurations used.

4.2. Monte Carlo Simulation. To complement the SCMFT, we have also performed Monte Carlo simulations with the same microscopic model as for the former, to have the possibility to compare results obtained from both methods. A box of volume 100^3 lattice sites with periodic boundary conditions was chosen. The Monte Carlo moves introduced to sample the phase-space are⁷³ chain reptation (chosen on average 80% of the times), configurational bias Monte Carlo type of chain growth (19.99%), and cluster moves (0.01%). In the cluster moves, and for the analysis of the aggregate size distributions, a surfactant is taken to be part of a cluster when one of the hydrophobic tail beads is in nearest-neighbor contact with at least one tail bead of another surfactant molecule belonging to the same cluster. The latter is therefore the definition of what we have considered as a cluster in this article.

The simulations were initiated with a random configuration of the surfactants, and 10^9 Monte Carlo steps were subsequently applied in order to make sure that the systems were correctly equilibrated. An additional production run of 10^{11} steps was then used in order to calculate the average properties of the system. Each simulation required approximately 10 days of computer time on a standard serial workstation.

Radius of Gyration. To investigate the shapes of the clusters of surfactants (ultimately the micelles), the principal radii of gyration were calculated by first evaluating the radius of gyration tensor, $R_{\alpha\beta}^2$, of each aggregate, defined as

$$R_{\alpha\beta}^2 \equiv \frac{1}{N_m} \sum_{k=1}^{N_m} (x_{\alpha,k} - x_{\alpha,i}^{\text{cm}})(x_{\beta,k} - x_{\beta,j}^{\text{cm}}) \quad (12)$$

where N_m is the total number of sites occupied by segments belonging to the aggregate, and $x_{\alpha,k}$ stands for any of the $\alpha = x, y, z$ spatial coordinates of the k th site of the aggregate. The superscript cm refers to the coordinates of the center of mass of the cluster.

The three principal radii of gyration are then calculated by diagonalizing the tensor. We furthermore ordered the eigenvalues $R_{1,2,3}$ so that $R_1 > R_2 > R_3$. These values characterize the size and shape of the micelle. For a cylinder, $R_1 > R_2 \approx R_3$, and for a sphere, $R_1 \approx R_2 \approx R_3$, while for a disk, $R_1 \approx R_2 > R_3$.

In addition, for every aggregate we introduced the ratios $\alpha = (R_2/R_1)^2$ and $\beta = (R_3/R_1)^2$, which contain all the relevant information about the shape of the cluster in only two appropriate parameters, as we will later see. Note that, by definition, α and β have values in the range (0,1). If both α and β are close to unity, this implies that all three principal radii of gyration are approximately equal, and the aggregate, therefore, has a shape close to that of a sphere. However, if α and β are close to zero, this implies that the first radius of gyration R_1 is much larger than the other two; thus, the aggregate has a cylindrical rodlike shape. Finally, if $\alpha \approx 1$ and $\beta \approx 0$, the shape of the aggregate will be a disk. The different geometric shapes of the aggregates can be conveniently distinguished in a 2D contour plot for the probability distribution for (α, β) . In Figure 1 we have visually indicated the shape that would correspond to a aggregate with a given (α, β) values. Other ways of characterizing micellar shapes can be found.^{74,75}

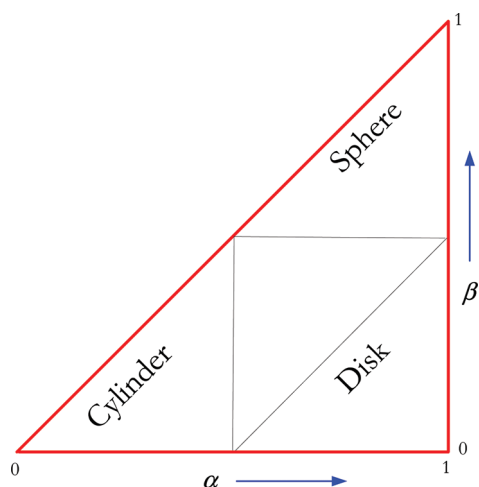


Figure 1. Schematic representation of the different geometric shapes of micelles as a function of the ratios of the principal radii of gyration, α and β .

5. RESULTS AND DISCUSSION

In this section, results will be presented for two surfactants, in order to emphasize the difference between a surfactant that prefers forming nearly spherical aggregates at all concentrations, as compared to a surfactant that undergoes a shape transition from spherical to cylindrical micelles. The surfactant chosen for the first case is the symmetric H_4T_4 surfactant. In the second case, the asymmetric H_3T_6 surfactant was chosen. Both 1D and 2D SCMFT calculations have been carried out along with Monte Carlo simulations, aimed at giving a detailed description of the shape transition.

5.1. The Symmetric Surfactant H_4T_4 . The standard chemical potential difference for 1D spherical and infinite

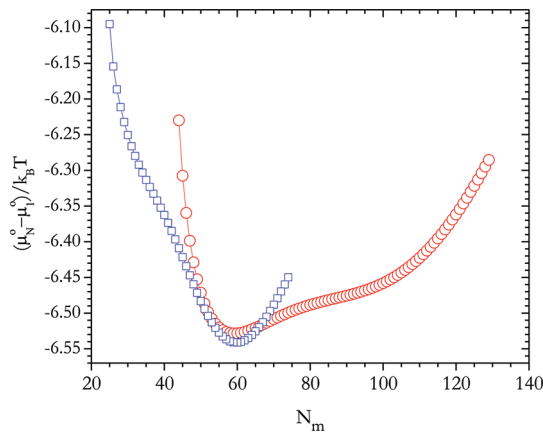


Figure 2. Standard chemical potential difference, $(\mu_N^{\circ} - \mu_l^{\circ})/k_B T$, for spherical micelles (squares) and for infinite cylindrical micelles (circles) of H_4T_4 , at dimensionless temperature $T^* = 7.0$ from 1D SCMFT calculations. In the case of the infinite cylindrical geometry, the x-axis gives the number of surfactants for a 19 lattice site section of the infinite cylinder.

cylindrical field geometries, at $T^* = 7.0$ for H_4T_4 are presented in Figure 2. It can be seen that the spherical micelle has a lower minimum in the standard chemical potential difference than the infinite cylindrical micelle, implying that H_4T_4 prefers forming spherical micelles.

2D SCMFT calculations have also been carried out for this system. The results were first checked against the 1D SCMFT standard chemical potential differences and other relevant properties such as density profiles, in order to validate the 2D results. Figure 3 shows the contour plots for the volume fraction profiles of the hydrophilic tail group for selected micelles of aggregation numbers, N_m , from 30 up to 110 chains. The volume fraction profiles are presented in terms of equal density contour plots, where the higher values of volume fraction are given in red and the lower in blue. The core of the micelles is predominantly occupied by the hydrophobic tail, while the hydrophilic head forms the corona of the micelle. We observe for this range of aggregation numbers that the micelles remain spherical and that they grow in size. This growth is due to the addition of more surfactants and is accompanied by the stretching of the tails to exclude the solvent from the inner core of the micelle. Due to this fact, this growth cannot go on without limit, forcing the system to divide into additional smaller spherical micelles, for the symmetric surfactant. In Figure 3 $N_m = 110$ already represents the biggest micelle that we have encountered from SCMFT. However, the previous conclusion arises from the analysis of the Monte Carlo results, since we have not gone to large enough aggregation numbers in order to be able to see two spherical micelles as a solution to the SCMFT.

Since there is a bulk concentration of surfactants in solution in equilibrium with the aggregate, not all the surfactants included in the simulation box are found in the aggregate. However, due to the low solubility of the surfactants, their number in the bulk is relatively small, even for the larger simulation box. Thus, if N is the total number of surfactants in the box, N_m , the aggregation number, is slightly smaller in all cases. In the SCMFT calculations we have estimated N_m by subtracting the bulk chain concentration times the total volume of the system from the total number of surfactants in the box N ; by proceeding in this way, we can compare results from different box sizes, which perfectly overlap when the results are plotted as a function of N_m .

Although a possible solution for the 2D SCMFT could be that of more than one aggregate, since such a solution can also satisfy the axisymmetric constraint of the field, we have always obtained solutions with one single aggregate. This is due to the fact that the interfacial energy as well as the geometric constraint of such small boxes hinders this possibility as a finite size effect. The standard chemical potential reaches a minimum at about 55 surfactant chains in the box⁷⁶ (not shown) and steadily increases for larger aggregates. It is thus expected that H_4T_4 should prefer to form spherical micelles, as expected from the analysis of the 1D solution. Indeed, this prediction is consistent with the analysis of the Monte Carlo simulations of the same system. Effectively, on calculating the ratios of the principal radii of gyration (Figure 4), it is found that the shape of the micelles remain approximately spherical as the surfactant concentration increases. It is interesting to note, however, that the distribution plot in Figure 4, for all concentrations, shows more likely fluctuations toward a cylindrical shape (extension along the $\alpha = \beta$ axis), rather than to disks.

The equilibrium micelle size distribution of Monte Carlo simulation, for the same system with overall volume fractions of surfactants of 0.016, 0.024, and 0.032, is shown in Figure 5. The micellar size distributions are smooth with a single peak at an aggregation number of about $N \approx 75$, independent of the total concentration of surfactants in the system. This indicates that,

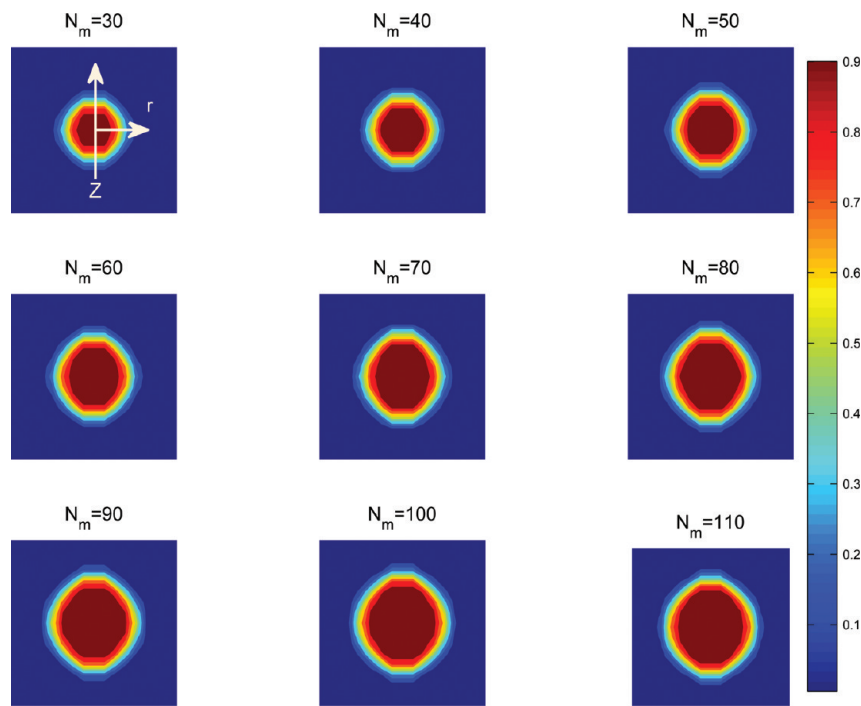


Figure 3. Volume fraction profile of the hydrophobic tails (ϕ_T), for the H₄T₄ surfactant at $T^* = 7.0$ of micelles of aggregation number N_m from 2D SCMFT calculations. From a simulation box of volume 17^3 and $N_{\text{bulk}} \approx 10$.

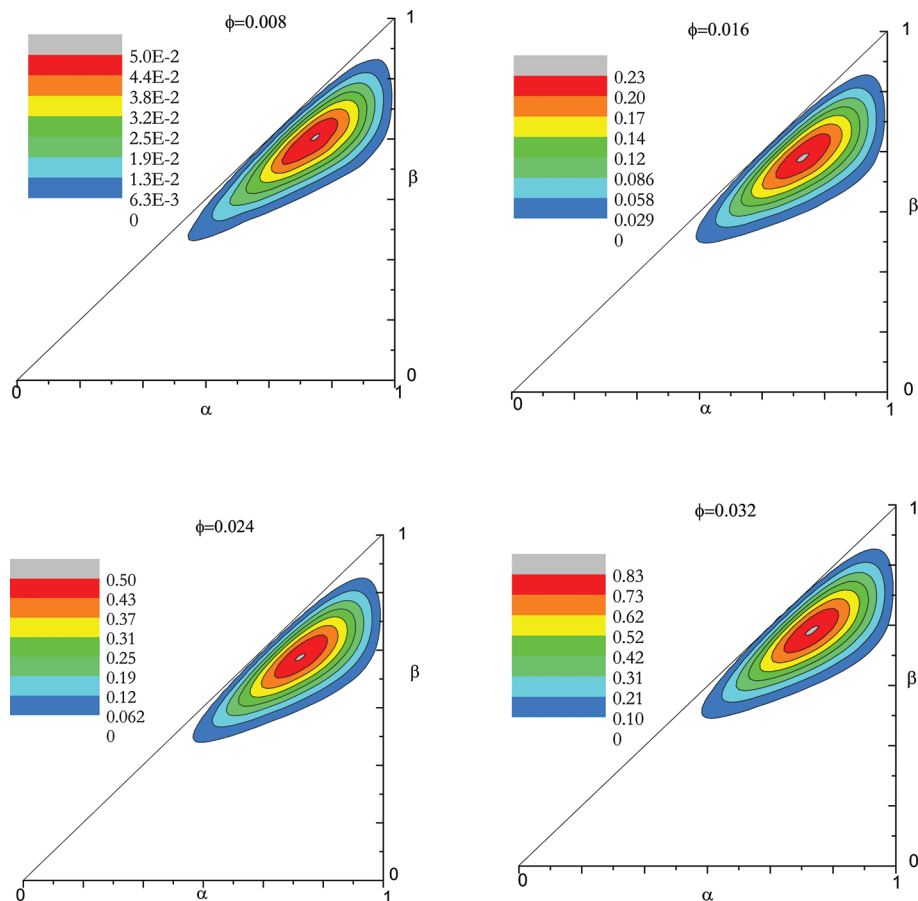


Figure 4. Contour plots of the distribution of the α/β radii of gyration ratios, for H₄T₄ at $T^* = 7.0$ for systems with chain volume fractions, ϕ , of 0.008, 0.016, 0.024, and 0.032, (containing 1000, 2000, 3000, and 4000 surfactants) from Monte Carlo simulations in a box of volume of 100^3 (see Figure 1).

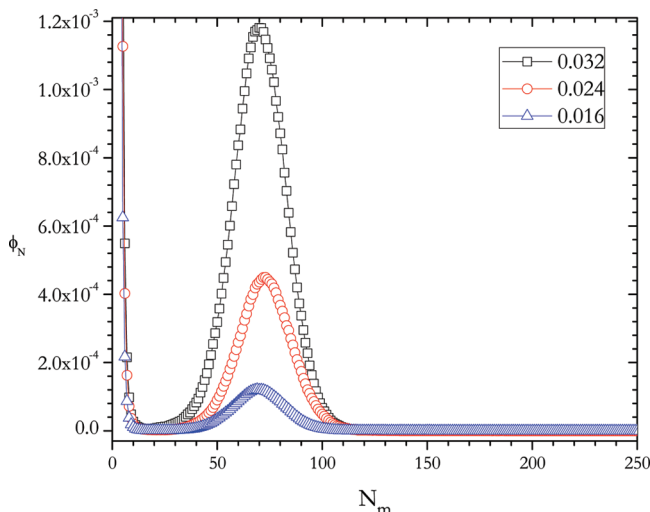


Figure 5. Micelle size distribution for H_4T_4 at $T^* = 7.0$ for systems with volume fractions 0.016, 0.024, and 0.032 from Monte Carlo simulations in a box of volume 100^3 .

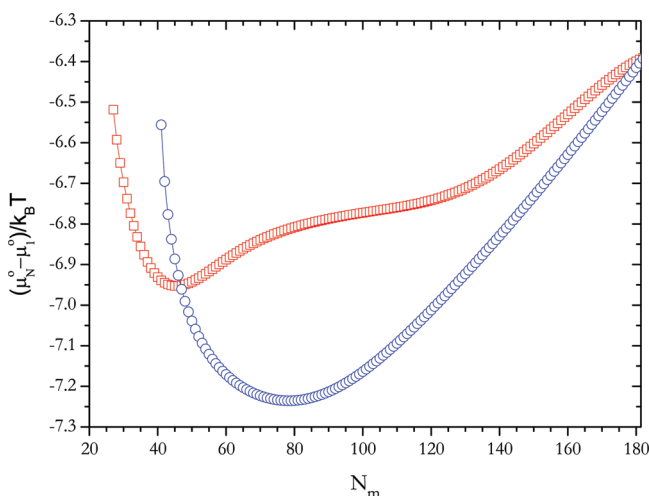


Figure 6. The standard chemical potential difference $(\mu_N^o - \mu_1^o)/k_B T$, of H_3T_6 versus N_m of spherical micelles (square) and infinite cylindrical micelles (circles) at $T^* = 9.5$ from 1D SCMFT calculations. In the case of the infinite cylindrical geometry, the x -axis gives the number of surfactants for a 19 lattice site section of the infinite cylinder.

on increasing the total number of surfactants, the system chooses to form more micelles of the same size, instead of gathering the additional surfactants in less energetically favorable larger aggregates. Furthermore, note that there is a significant difference between the aggregation number at the peak obtained from the Monte Carlo simulations, 75, as compared to the aggregation number found at the minimum of the standard chemical potential, from the SCMFT calculations, about 55 chains. This difference between the mean-field theory and simulation can be attributed to various factors, with the lack of number fluctuations in the mean-field at the forefront. In any case, the consistency of the two procedures strongly indicates the correctness of the conclusion that the symmetric surfactant studied only forms spherical micelles.

5.2. The Asymmetric Surfactant H_3T_6 . The results of the SCMFT for the standard chemical potential difference, $(\mu_N^o - \mu_1^o)/k_B T$ versus the total number of surfactants in the system,

N_m , at a dimensionless temperature $T^* = 9.5$ are shown in Figure 6 for the 1D spherical and infinite cylindrical field geometries. As can be observed in the figure, the infinite cylindrical micelle has a lower minimum in the standard chemical potential than that of the spherical case. This indicates that the infinite cylindrical micelle has a lower formation energy per surfactant than the spherical micelle, for the aggregation numbers that correspond to the minima of these curves. The 2D SCMFT permits us to see how the standard chemical potential of the different aggregate shapes changes between the two limiting cases given by the 1D analysis. The study is complemented with the results obtained from the Monte Carlo simulations of the same system. Again, the standard chemical potential differences, when 1D geometry is imposed on to the 2D procedure, are in quantitative agreement with the infinite cylinder and sphere results from the 1D calculations.

Volume fraction contour plots of tail segments of micelles of aggregation numbers, N_m , equal to 40, 60, 80, and 100, in a simulation box of $V = 27^3$, together with simulations of N_m equal to 110, 130, 150, 170, and 210 in a bigger simulation box of $V = 35^3$ are shown in Figure 7. The higher values of volume fraction are given in red and the lower in blue.

One can see how in this case the micelle evolves from a spherical to a finite size cylindrical micelle as N_m increases. At lower aggregation numbers, distinctly spherical micelles are preferred, as is the case for $N_m = 40$. The spherical micelle undergoes a first shape transition by starting to elongate in the z -axis, forming a prolate ellipsoid up to $N_m \approx 110$. In this sequence, the eccentricity of the micelle increases by increasing faster in the z -axis with respect to that of the cross section.⁷⁶ As can be seen in the same Figure 7, for aggregation numbers $N_m \approx 130$ and larger, the prolate ellipsoid undergoes a second shape transition by developing a concave contour, anticipating that the preferred form for very large aggregation numbers will be that of a capped cylinder, as was convincingly argued by Eriksson²¹ and others,^{9,53} where the hemispherical end-caps have a larger diameter than the cylindrical body. The radius of the caps are significantly larger than the most stable sphere ($N_m \approx 80$ as compared to $N_m \approx 40$), while the body of the object has a diameter that coincides with the preferred diameter of the infinite cylinder 1D result. With regards to ref 11, where it was conjectured that the capped cylinder should inherit the diameters corresponding to the most stable sphere and cylinder, the actual solution of the SCMFT in two dimensions indicates that the caps are strongly influenced by the junction with the cylindrical body, as to force these end-caps to a size that is not the one that would be preferred by an isolated sphere. Nevertheless, the cylindrical body does comply with a diameter that is the same as for the infinite cylinder. Thus we can conclude that, for this kind of surfactant, the tendency to form cylindrical objects seems to be the dominant effect to explain the shapes that we encounter in our calculations.

Since the limit of the spherical packing of the hydrophobic parts of the surfactant is already achieved in the hemispherical end-caps, further addition of surfactants to such a micelle does not lead to the reconstruction of the end-caps; instead, they participate in elongating the cylindrical part of the micelle. In our lattice model, the length of the cylindrical part of the micelle increases by 1 lattice unit with the addition of approximately eight extra surfactants. Thus, the length L of the object can be approximated by $L \approx (N_m - 80)/8 + 14$, for aggregates larger than 80. Obviously, the 2D SCMFT solution of the field equations does not take into account the fact that

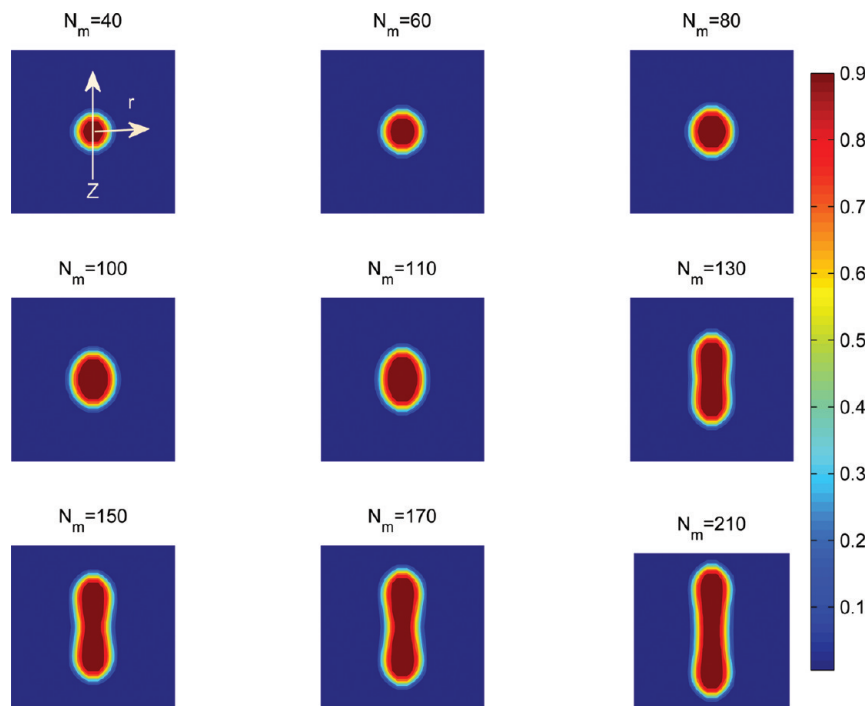


Figure 7. Volume fraction profiles of the hydrophobic tails of micelles of H_3T_6 at $T^* = 9.5$ from 2D SCMFT calculations for selected micelles of aggregation number N_m , from simulation boxes of 27^3 ($N_m = 40, 60, 80, 100$) and 35^3 ($N_m = 110, 130, 150, 170, 210$). Note that the same 35×35 scale is used for all plots to allow a direct comparison of the aggregates.

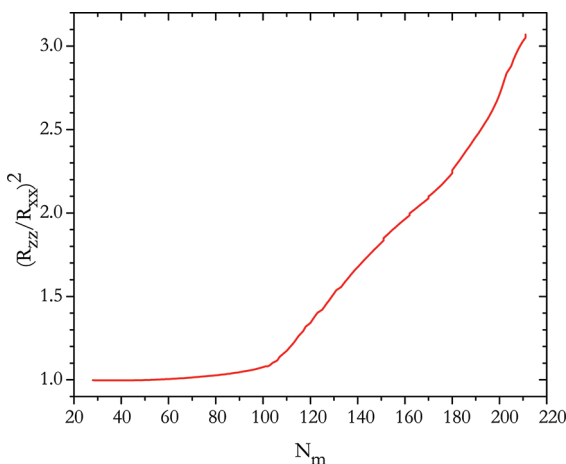


Figure 8. Variation of the ratio of the principal radii of gyration $(R_{zz}/R_{xx})^2$, with the aggregation numbers of micelles, N_m , for the H_3T_6 surfactant at $T^* = 9.5$ from 2D SCMFT calculations; values for $N_m < 105$ are obtained from a simulation box of volume $V = 27^3$ and $N_m > 105$ for $V = 35^3$.

very long cylindrical micelles will bend due to thermal agitation, producing curved objects, such as those that we observed in the MC simulations, as discussed later on.

To characterize the different shapes of the micelles, we have calculated the different radii of gyration (defined by eq 12). First of all, the symmetry of the object ensures that the matrix of radii of gyration is diagonal. Furthermore, since the fields have a symmetry of revolution, $R_{xx} = R_{yy}$. We thus plot the ratio of the square of the radii of gyration in the z -axis with respect to that in the x -axis. If this ratio is approximately equal to 1, this indicates that spherical aggregates are formed, whereas values larger than 1 are indicative of cylindrical aggregates. Finally,

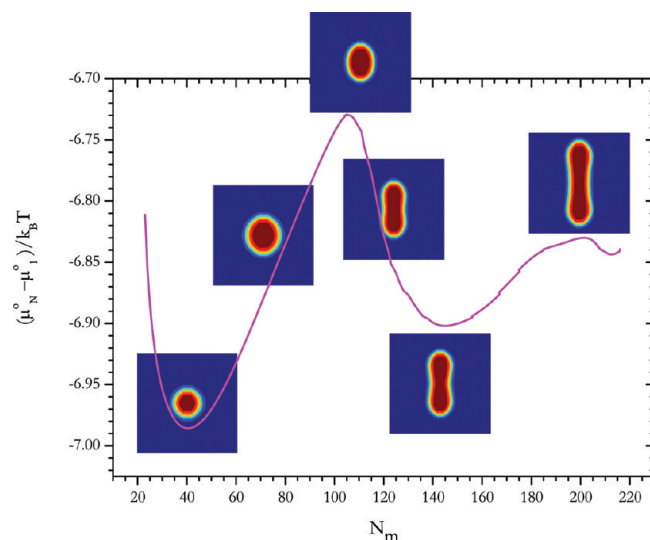


Figure 9. Micellar shape transition along with the standard chemical potential differences $(\mu_N^o - \mu_1^o)/k_B T$ versus the micellar aggregation number of the micelle, N_m , at a dimensionless temperature $T^* = 9.5$ from 2D SCMFT calculations. The inserted contour plots are for $N_m = 40, 80, 110, 125, 140$, and 200 .

values less than 1 would indicate the presence of disklike aggregates.

In Figure 8, we see that the value of $(R_{zz}/R_{xx})^2$ increases with the size of the micelle, especially for $N_m > 100$, indicating that the micelle elongates in the direction of the z -axis. This plot supports the visual evidence from the volume fraction profiles already given in Figure 7.

As has been mentioned, the major advantage of the SCMFT with regard to MC simulations is the ease of calculation of properties related to the free energy of the system. In our

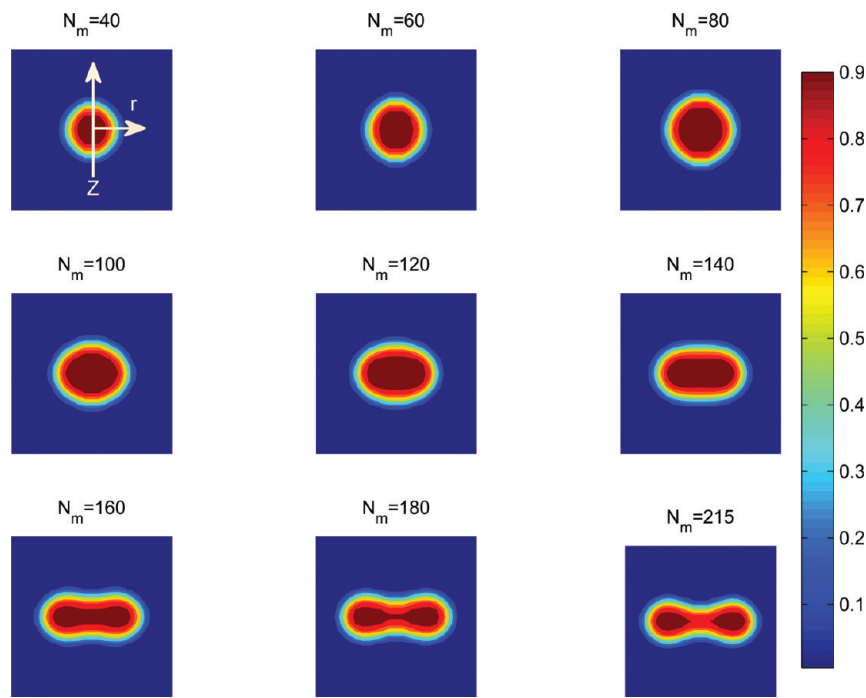


Figure 10. Volume fraction profiles of the hydrophobic tail are presented for selected micelles of aggregation numbers N_m showing the sphere to disk transition of micelles of H_3T_6 surfactants at $T^* = 9.5$ from 2D SCMFT calculations, in a cubic box of volume, $V = 25^3$.

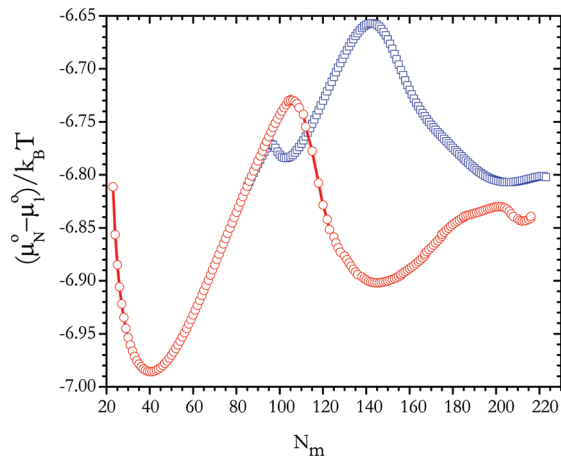


Figure 11. The standard chemical potential differences, $(\mu_N^o - \mu_1^o)/k_B T$, vs N_m , of H_3T_6 surfactants at $T^* = 9.5$ for the sphere to disk (squares) and sphere to cylinder (circles) shape transitions from 2D SCMFT calculations.

analysis, the relevant thermodynamic quantity is the standard chemical potential difference. In particular, we can determine $(\mu_N^o - \mu_1^o)/k_B T$, which represents the difference in free energy cost of introducing one surfactant in the simulation box, containing the micelle in its center, as compared to the reference state. Similar to the 1D SCMFT,⁷⁶ the 2D SCMFT calculations of the standard chemical potential are found to be box-size-independent.

One of the most important results of this work is presented in Figure 9, where the standard chemical potential is shown as a function of the aggregation number. Every point in the curve refers to a given micelle with the corresponding aggregation number, as obtained one by one from our simulations. The fact that we have constrained the size of the box to be small only allows one micelle to form at any one time inside the system, in

a way that permits us to significantly change the chemical potential through the number of surfactants in the box N . In this way we can explore the whole curve by quasicontinuously varying the aggregation number and simultaneously measuring the standard chemical potential. Therefore, the fact that the minimum is at $N_m \approx 40$ indicates that this will be the most stable size. In other words, if one prepares a system with a larger volume and a larger number of surfactants, many micelles would coexist, with different sizes, whose number would be determined by their difference in standard chemical potential, where the spherical ones would be the most frequent.

Once we have clarified the meaning of the curve in Figure 9, one can analyze its particular profile. First, we have already mentioned the existence of the deepest minimum for a spherical micelle of about $N_m \approx 40$. For larger aggregation number we find a secondary minimum at $N_m \approx 145$, when the elongated micelle develops two distinct hemispherical end-caps. The energetic barrier between these minima corresponds to the penalty that the system has to pay to allocate more surfactants in a bigger micelle without significantly changing its shape, compromising the screening of the hydrophobic core from the external solvent. Such an ellipsoidal conformation has a large energetic penalty due to the curvature of the surface. Thus, it seems rather obvious that the system should change its shape after the maximum to accommodate more surfactants and seeks for the preferred curvature of the surface. Second, for larger aggregation numbers, we see another energetic barrier that seems to separate the studied region from another energy valley that seems to develop at about $N_m \approx 215$. Although we cannot be conclusive about the existence of such additional valleys at large aggregation number, such behavior is in agreement with the results of May and Ben-Shaul,⁵³ Jódar-Reyes et al.,⁹ and Leermakers et. al.⁷⁷ who pointed out that the grand potential^{9,77} and packing energy⁵³ of the cylindrical micelle has an oscillatory behavior with an amplitude that decays with the length of the cylinder, showing that the cylindrical part

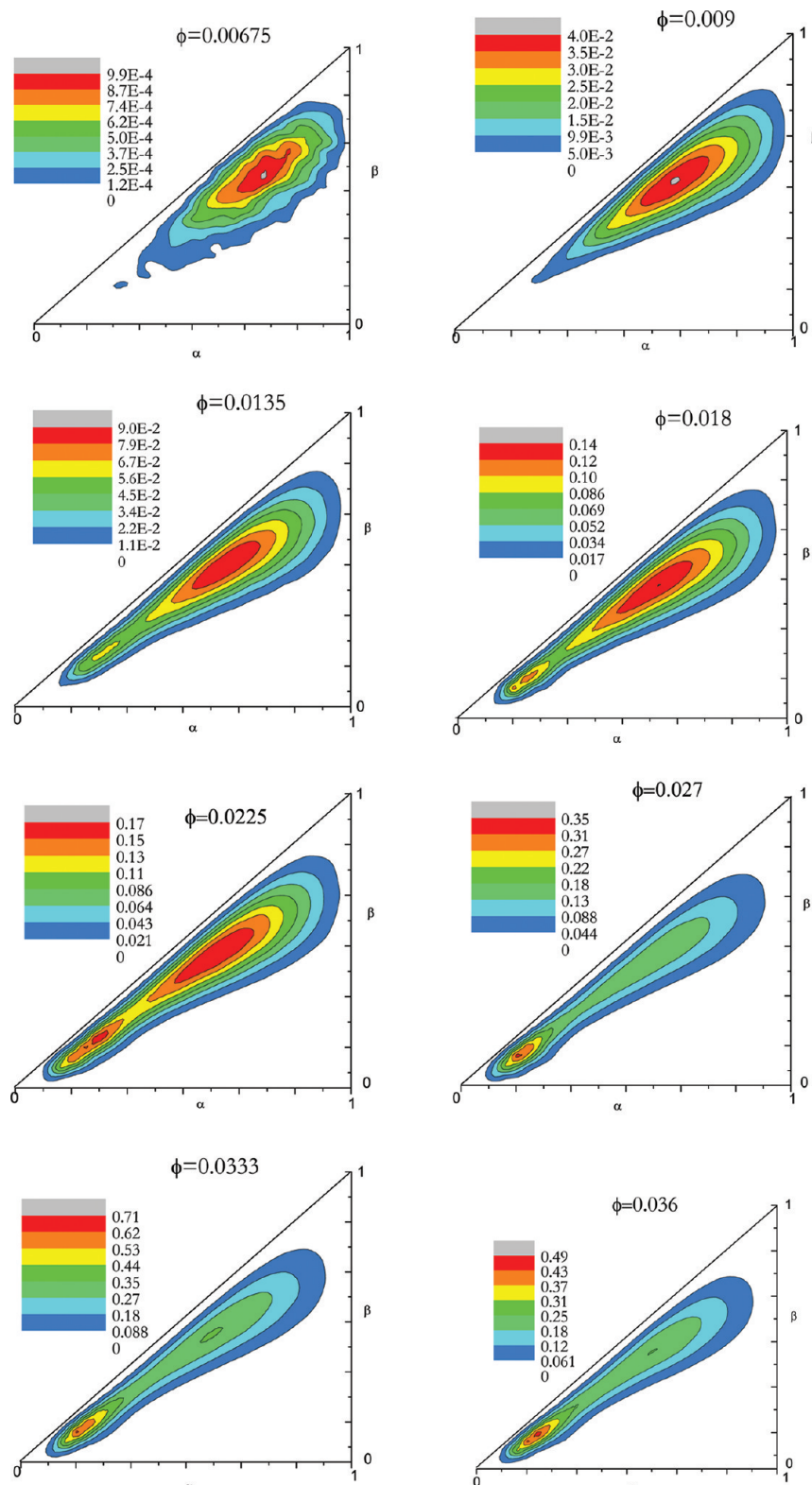


Figure 12. Contour plots of the distribution of the α and β radii of gyration ratios for H_3T_6 surfactants at $T^* = 9.5$, for the systems with volume fractions (ϕ) of 0.00675, 0.009, 0.0135, 0.018, 0.0225, 0.027, 0.033, and 0.036 (containing 750, 1000, 1500, 2000, 2500, 3000, 3700, and 4000 surfactants) from Monte Carlo simulations in a box of volume 100^3 . The sphere to cylinder shape transition occurs through a region where they exist together with some other intermediate shapes (see Figure 1).

must have a minimum length to avoid strongly unfavorable interferences between the end-caps.

Porte et al.⁷⁸ suggested long ago that there should be a gap in the size distribution of wormlike micelles, between the spherical

micelles and the long micelles, because of the more unfavorable state of the surfactants that are at the junction between the cylindrical body and the end-caps, i.e., at the neck of the micelle. From our curves, and in agreement with our reasoning

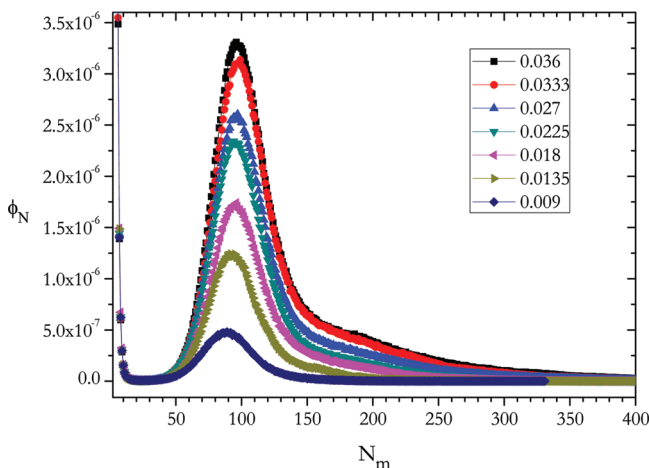


Figure 13. Micellar size distribution for H_3T_6 surfactants at $T^* = 9.5$ with volume fractions of 0.009, 0.0135, 0.018, 0.0225, 0.027, 0.0333, and 0.036 from Monte Carlo simulations in a box of volume 100^3 .

above, we see that the system would prefer forming either spherical micelles with size around $N_m \approx 40$, with size fluctuations, or capped cylinders of a size near $N_m \approx 140$, with fluctuations, better than quasispherical micelles of about $N_m \approx 100$.

Finally, one has to realize that the curve of standard chemical potential as given in Figure 9 should decrease with the aggregation number until meeting the limit of the infinite cylinder, as given from the 1D calculations in Figure 6, corresponding to $(\mu_N^0 - \mu_1^0)/k_B T \simeq -7.25$. This is significantly below the values found for the finite cylinder and should be approached in the asymptotic limit of large aggregation numbers, where the hemispherical end-caps have a negligible contribution to the overall micelle.

Besides the standard or conventional pathway for the sphere to rod transition, where the amphiphilic molecules first self-assemble into small spherical micelles and then elongate to cylindrical micelles, as discussed above, the SCMFt calculations reveal the existence of an alternative pathway toward the infinite cylinder, that is, by way of a doughnut-like or torus shape for the micelle. Obviously, by increasing the radius of the hole of such a shape, one also approaches the limiting situation, with the additional advantage of forming no caps in the intermediate regime. However, such a shape is hampered by the curvature of the surface, at least at the initial stages. Our calculation shows a bifurcation in the standard chemical potential plot, as indicated in Figure 11. The micelles that give rise to the additional branch are initially disklike or oblate spheroidal and evolve toward a red-blood-cell-like shape that precedes the formation of the hole and then the doughnut-like shape alluded to above (see Figure 10). Notice, in addition, that for large aggregation numbers, where the effects of the curvature as well as the end-caps lose relative importance, the standard chemical potential of both shapes, prolate and oblate, tend to very close values. We have not continued the simulation further in aggregation number due to the large systems required. Nevertheless, nothing precludes the possibility that the doughnut-like shape would end up having lower standard chemical potential than the capped rod.

The existence of the bifurcation in the shape transition is one of the most important results of this work.

Therefore, according to Figure 11, where both branches are plotted, the transition pathway is richer than previously

assumed. We locate the bifurcation point at an aggregation number of $N_m \approx 95$. The micelles with $N_m < 95$ are slightly prolate. From this point on the system has to choose between continuing the elongation with a prolate shape, which increases the standard chemical potential, or choosing the other branch and suddenly become oblate. In the oblate branch, a small minimum is reached at about $N_m \approx 100$, to increase up to a maximum that occurs later and is higher than that of the prolate branch. Then, the energy decreases by forming a depletion in the symmetry axis, which grows in size and depth as we increase the aggregation number. This process has evident similarities with the one already discussed for a decrease of the standard chemical potential of the prolate branch when the two end-caps form. Finally, the energy of both branches approach each other at about $N_m \simeq 200$.

In summary, the SCMFt free energy calculations suggest that in a large system with an overall surfactant concentration significantly above the cmc, one should expect that many spherical micelles of N_m around the minimum form, with some capped cylindrical micelles with much larger aggregation numbers, but also a few disklike micelles.

In order to complete our analysis, Monte Carlo simulations for this system have been carried out using the same model H_3T_6 . Compared to the SCMFt calculations, we have used larger boxes with a concentration above the cmc. Therefore, objects with larger standard chemical potential are very unlikely to be seen in the system, due to the fact that the increase of the overall concentration in the system produces more aggregates but keeps the bulk concentration close to the cmc.

The shape transition occurs from spherical micelle to cylindrical micelles through a region where both spheres and cylinders coexist. The coexistence of spherical and cylindrical micelles has also been supported with experimental results using cryo-TEM and pulse gradient spin-echo NMR³⁷ and simulations.^{57,59}

We present simulation results for systems with global volume fractions ϕ equal to 0.00675, 0.009, 0.0135, 0.018, 0.0225, 0.027, 0.0333, and 0.036 (containing 750, 1000, 1500, 2000, 2500, 3000, 3700, and 4000 surfactant molecules, respectively) in a simulation box of volume 100^3 lattice sites. The contour plots of the distribution of the parameters α and β , describing the ratios of the principal axis of gyration, are shown in Figure 12. At low concentrations predominantly spherical micelles are formed, similar to the H_4T_4 surfactant case. However, for the H_3T_6 , at $\phi = 0.0135$ we can already observe a small peak in the region of the cylindrical shapes. The formation of these two peaks is indicative of the coexistence between the spherical and cylindrical micelles. At larger concentrations, the system mostly generates elongated aggregates. It is interesting to remark that in the intermediate concentrations $\phi = 0.0135-0.0333$ the saddle point between the peaks is maintained, in agreement with the existence of an energetic barrier between the sphere and the capped cylinder, as discussed above.

The equilibrium volume fraction of micelles of a given aggregation number for the same systems discussed above is shown in Figure 13. As can be observed, the micellar size distributions are smooth with a peak and a noticeable shoulder at higher aggregation numbers, in the case of systems with higher total volume fractions. Notice, however, that with respect to the SCMFt calculations, the most probable aggregate obtained in the MC simulations corresponds to a sphere of about $N_m = 90$, about twice the aggregation number of the minimum of the energy landscape obtained with the

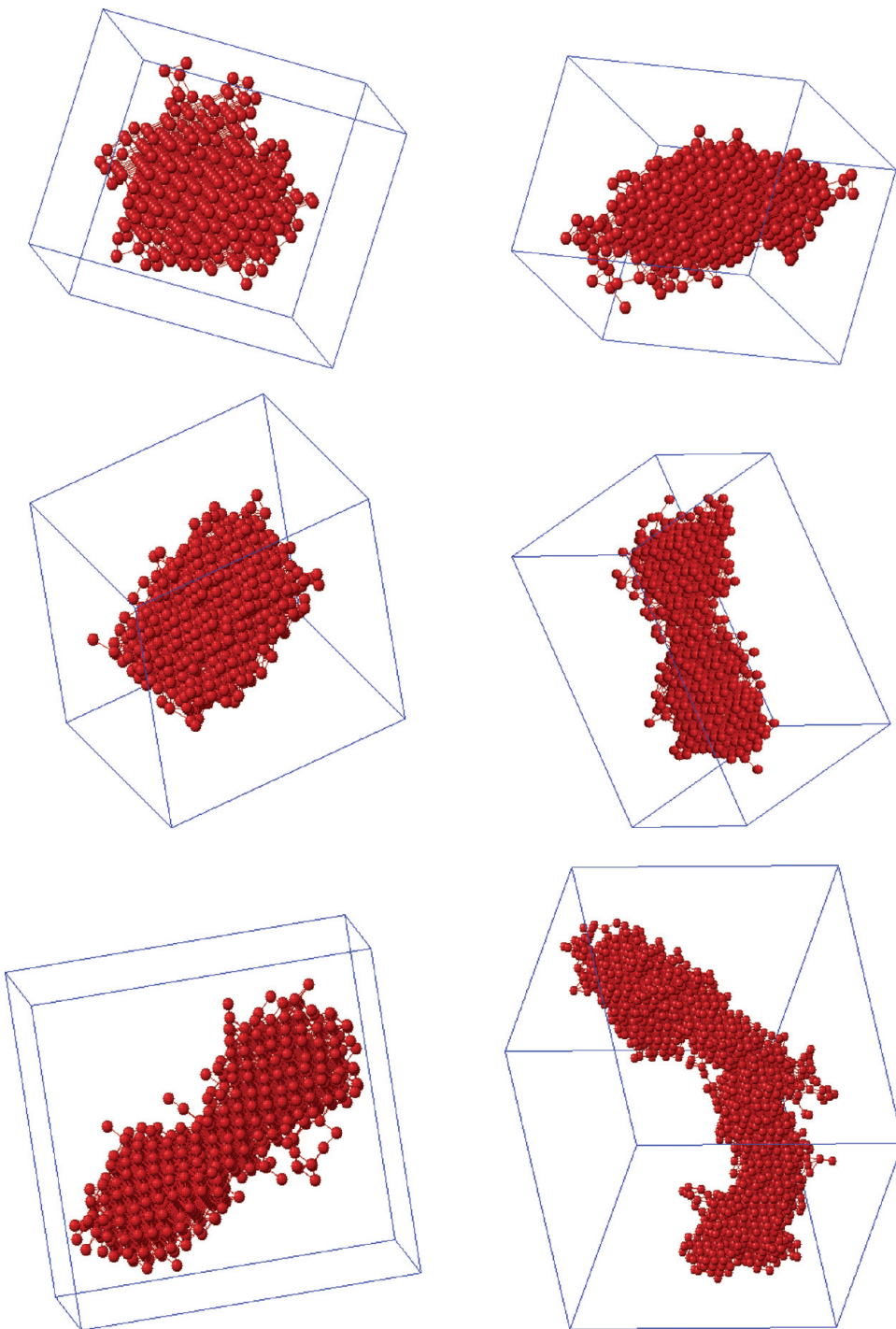


Figure 14. Snapshots of micelles of different geometric shapes obtained from Monte Carlo simulation showing the sphere to cylinder transition: (left to right) sphere, $N_m = 90$; ellipsoidal, $N_m = 110$; croquette micelles, $N_m = 129$; dumbbell cylindrical micelles, $N_m = 130$ and $N_m = 160$; and long cylindrical micelles, $N_m = 350$. Note that the boxes shown are just a guide for the eye, the simulation box is 100^3 .

SCMFT. This is a known effect already mentioned in the previous section for the symmetric surfactant. The presence of the rodlike aggregates can also be seen in the existence of the shoulder of Figure 13 at large total volume fraction. Again, the size of the cylindrical aggregates is larger than those predicted in the SCMFT. Notice, in addition, that the size distribution from the SCMFT can be constructed combining the mass action model together with the standard chemical potential difference found in Figure 11. At sufficiently large chemical potential, this model yields separate peaks corresponding to the

minimum energy objects and their fluctuations, namely, spheres and cylinders separated by a gap in size, instead of the shoulder observed in Monte Carlo simulations, as expected from mean-field calculations. Therefore, the information given by SCMFT is of great value, although qualitative when the goal is a full comparison with simulation of experimental results. This is particularly noticeable for this type of soft matter systems for which the differences in free energy of the different objects that can coexist is only a fraction of a kT .

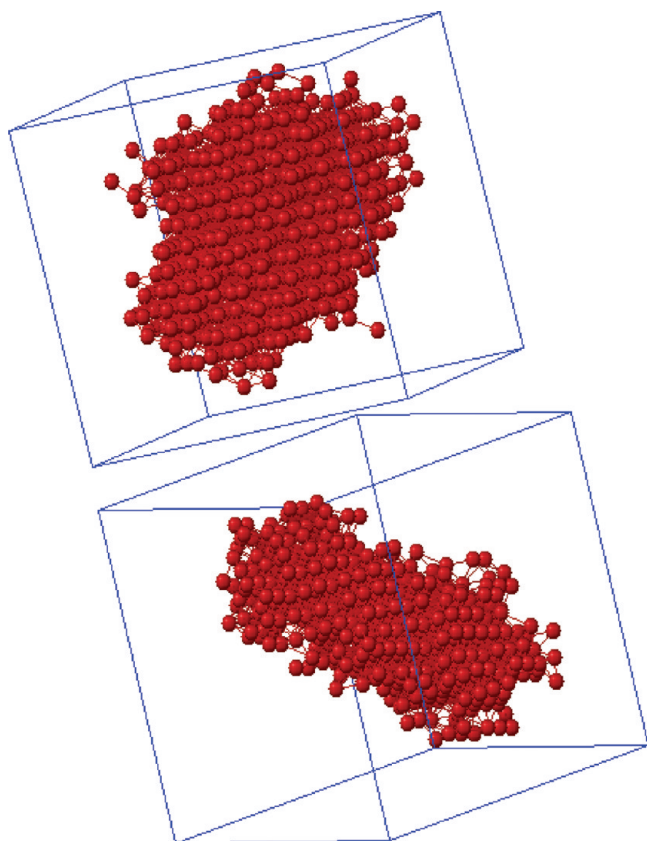


Figure 15. Snapshots of disk micelles, obtained from Monte Carlo simulations for aggregation numbers $N_m = 121$, presented with top and side views. Note that the boxes shown are just a guide for the eye. The simulation box is 100^3 .

Direct evidence of the rodlike shapes existing in the system can be found in Figure 14. It is interesting to observe the caps of the rod in several individuals, as well as the bending encountered for longer rodlike aggregates. Finally, we have also occasionally observed disklike aggregates (Figure 15), in agreement with the bifurcation found in the SCMFt calculations. It should be noted that these aggregates correspond to the lower part of the middle of the contour distribution plot in Figure 12.

6. CONCLUSIONS

We have studied the shape transition of micelles, induced by the increase of surfactant concentration, in model systems representing a symmetric as well as an asymmetric surfactant. The symmetry refers to the relative size of the head to the tail segments of the surfactants, which varies the tendency of a given system to have a preferred curvature. The method of analysis is to combine SCMFt calculations to obtain a good description of the energetic behavior of the system, with MC simulations that guarantee a proper solution of the statistical mechanical problem of a system of many micelles coexisting in a system. The predictions of the mean-field method can then be compared to the results of the MC simulations and validate the dependency of the standard chemical potential curve with regard to the aggregation number, especially at large aggregate size.

We have observed that the symmetric surfactant H_4T_4 is only able to form spherical micelles over a large range of chemical potential values. Furthermore, the infinite cylinder has a

standard chemical potential larger than the spherical micelle. The MC simulations for this case produce only spherical micelles, in agreement with the SCMFt calculations. Large objects are not observed due to the tendency of the system to multiply the number of spherical micelles when the number of surfactants is increased in the system. These results are in agreement with other works where it is also stated that symmetric surfactants give only spherical micelles under similar conditions as those studied here.

On the other hand, we have also analyzed the asymmetric surfactant H_3T_6 . In this case, the SCMFt calculations of one-dimensional objects clearly indicate that the standard chemical potential of the infinite cylinder is lower than that of the most favorable spherical micelle. This, by itself, is a clear indication that this type of system will eventually evolve toward elongated objects, even at moderately low surfactant concentration (correspondingly, the low chemical potential of the system). In this, the asymmetric case is completely different from the symmetric surfactant, where the 1D SCMFt calculations indicate that the cylinder has a significantly larger standard chemical potential than the sphere. Indeed, the 2D SCMFt calculations for the asymmetric surfactant have revealed a fascinating standard chemical potential landscape, presenting a bifurcation between capped cylinders and red-blood-cell-like oblate shapes, never described before, to the best of our knowledge. More interestingly, the MC simulations show the occurrence of such disklike objects in the same type of simulations as in the symmetric case. This is, therefore, a strong argument in favor of the real existence of such a bifurcation in this kind of surfactants.

The transition between spheres to nonspherical objects is produced in this case always through the formation of a prolate ellipsoid on average, with an increase of the energetic cost of the formation of these objects. Moreover, our calculations seem to indicate that some sort of oscillation in the standard chemical potential profile can take place as the length of the cylinder increases, as has been documented in the literature. Furthermore, the branch of the oblate objects seem to be a different route toward the infinite cylinder. Effectively, a toruslike micelle, with a hole in its center, would be similar to a bent cylinder closed in on itself and, therefore, without the cost of developing end-caps. As chemical potential increases (increase of the free surfactant concentration in a canonical ensemble), we see that capped cylinders are preferred to oblate geometries. This can be seen from Figure 11 from the fact that the oblate branch has substantially higher standard chemical potential difference than capped cylinders of different aggregation numbers. Monte Carlo simulations are in agreement in the sense that in the big box the canonical simulation keeps the chemical potential low by creating additional aggregates that coexist with a certain probability proportional to its standard chemical potential difference. The populations found indicate that a large number of spheres coexist with elongated objects of different sizes and only occasionally the oblate objects appear, again proving that their energy of formation is significantly larger than the more common aggregates, at least at this low chemical potential. It would be interesting to continue our analysis beyond the sizes that have been covered with our current computer facilities.

To conclude, we expect that the analysis that we present is a suitable starting point for a deeper understanding of the problem of the self-assembly of amphiphilic molecules, especially with regard to the practical uses of objects of that

842 nature, whose shape could eventually be tailored at will, for
843 specific applications.

844 ■ AUTHOR INFORMATION

845 Corresponding Author

846 *E-mail: allan.mackie@urv.cat.

847 Notes

848 The authors declare no competing financial interest.

849 ■ ACKNOWLEDGMENTS

850 The authors acknowledge financial help from the Spanish
851 Ministry of Science and Innovation MICINN via project
852 CTQ2008-06469/PPQ.

853 ■ REFERENCES

- 854 (1) Israelachvili, J. *Intermolecular and Surface Forces*, 7th ed.;
855 Academic Press: San Diego, CA, 1998.
- 856 (2) Holmberg, K.; Jonsson, B.; Kronberg, B.; Lindman, B. *Surfactants*
857 and *Polymers in Aqueous Solution*, 2nd ed.; John Wiley & Sons, Ltd:
858 New York, 2002.
- 859 (3) Rosen, M. J. *Surfactants and Interfacial Phenomena*; John Wiley &
860 Sons, Ltd: New York, 2004.
- 861 (4) Hamley, I. W. *Introduction to Soft Matter: Synthetic and Biological*
862 *Self-Assembling Materials*; John Wiley & Sons, Ltd: New York, 2007.
- 863 (5) Mittal, K. L.; Shah, D. O. *Adsorption and aggregation of surfactants*
864 in solution; Marcel Dekker, Inc.: New York, 2003.
- 865 (6) Schramm, L. L. *Surfactants: Fundamentals and Applications in the*
866 *Petroleum Industry*; Cambridge University Press: New York, 2000.
- 867 (7) Puvvada, S.; Blankschtein, D. *J. Phys. Chem.* **1992**, *96*, 5579–
868 5592.
- 869 (8) Sterpone, F.; Briganti, G.; Pierleoni, C. *Langmuir* **2009**, *25*,
870 8960–8967.
- 871 (9) Jódar-Reyes, A. B.; Leermakers, F. A. M. *J. Phys. Chem. B* **2006**,
872 *110*, 6300–6311.
- 873 (10) Gonzalez-Perez, A.; Varela, L.; Garcia, M.; Rodriguez, J. *J.*
874 *Colloid Interface Sci.* **2006**, *293*, 213.
- 875 (11) Al-Anber, Z. A.; Bonet-Avalos, J.; Floriano, M. A.; Mackie, A. D.
876 *J. Chem. Phys.* **2003**, *118*, 3816–3826.
- 877 (12) González-Pérez, A.; Russo, J. M. *Colloids Surf., A* **2010**, *356*, 84–
878 88.
- 879 (13) Ulmius, J.; Wennerstroem, H.; Johansson, L. B. A.; Lindblom,
880 G.; Gravsholt, S. *J. Phys. Chem.* **1979**, *83*, 2232–2236.
- 881 (14) Chauhan, M.; Kumar, G.; Kumar, A.; Sharma, K.; Chauhan, S.
882 *Colloids Surf.* **2001**, *180*, 111–119.
- 883 (15) Panchal, K. N.; Desai, A.; Nagar, T. *J. Dispersion Sci. Technol.*
884 **2006**, *27*, 963–970.
- 885 (16) Kohler, H. H.; Strnad, J. *J. Phys. Chem.* **1990**, *94*, 7628–7634.
- 886 (17) Blokhuis, E. M.; Sager, W. F. C. *J. Chem. Phys.* **2001**, *115*, 1073–
887 1085.
- 888 (18) Goel, T.; Kumbhakar, M.; Mukherjee, T.; Pal, H. *J. Photochem.*
889 *Photobiol., A* **2010**, *209*, 41–48.
- 890 (19) Ozeki, S.; Ikeda, S. *J. Colloid Interface Sci.* **1980**, *77*, 219–231.
- 891 (20) Debye, P.; Anacker, E. W. *J. Phys. Colloid Chem.* **1951**, *55*, 644–
892 655.
- 893 (21) Eriksson, J. C.; Ljunggren, S. *J. Chem. Soc. Faraday Trans.* **1985**,
894 *2*, 1209–1242.
- 895 (22) Molina-Bolívar, J.; Aguiar, J.; Peula-García, J. M.; Ruiz, C. C. J.
896 *Phys. Chem. B* **2004**, *108*, 12813–12820.
- 897 (23) Rodriguez, A.; del Mar Graciani, M.; Bitterman, K.; Carmona, A.
898 T.; Moya, M. L. *J. Colloid Interface Sci.* **2007**, *13*, 542–550.
- 899 (24) Denkova, S. P.; Lokeren, L. V.; Verbruggen, I.; Willem, R. J.
900 *Phys. Chem.* **2008**, *112*, 10935–10941.
- 901 (25) Stigter, D. *J. Phys. Chem.* **1966**, *70*, 1323–1325.
- 902 (26) Miura, M.; Kodama, M. *Bull. Chem. Soc. Jpn.* **1972**, *45*, 2265–
903 2269.
- 904 (27) Burke, S. E.; Eisenberg, A. *Langmuir* **2001**, *17*, 6705–6714.
- 905 (28) Hayashi, S.; Ikeda, S. *J. Phys. Chem.* **1980**, *84*, 744–751.
- (29) Herrmann, K. W. *J. Phys. Chem.* **1964**, *68*, 1540–1546. 906
- (30) Attwood, D.; Terreros, A.; Lopez-Cabarcos, E.; Galera-Gomezy, P. A. *J. Colloid Interface Sci.* **2001**, *235*, 247–250. 907
- (31) Kodama, M.; Kubota, Y.; Miura, M. *Bull. Chem. Soc. Jpn.* **1972**, *45*, 2953–2955. 908
- (32) Kato, T.; Kanada, M.-A.; Seimiya, T. *J. Colloid Interface Sci.* **1996**, *181*, 149. 912
- (33) Cirkel, P. A.; Koper, G. J. M. *Langmuir* **1998**, *14*, 7095–7103. 913
- (34) von Berlepsch, H.; Dautzenberg, H.; Rother, G.; Jäger, J. *Langmuir* **1996**, *12*, 3631–3625. 915
- (35) Bernheim-Groswasser, A.; Zana, R.; Talmon, Y. *J. Phys. Chem. B* **2000**, *104*, 4005–4009. 916
- (36) Bernheim-Groswasser, A.; Wachtel, E.; Talmon, Y. *Langmuir* **2000**, *16*, 4131–4140. 918
- (37) Khan, A.; Kaplun, A.; Talmon, Y.; Hellsten, M. *J. Colloid Interface Sci.* **1996**, *181*, 191–199. 920
- (38) Zheng, Y.; You-Yeon, W.; Bates, F. S.; Davis, H. T.; Scriven, L. E.; Talmon, Y. *J. Phys. Chem. B* **1999**, *103*, 10331–10334. 922
- (39) Lin, W.; Zheng, C.; Wan, X.; Liang, D.; Zhou, Q. *Macromolecules* **2010**, *43*, 5405–5410. 924
- (40) Lee, S. J.; Park, M. J. *Langmuir* **2010**, *26*, 17827–17830. 926
- (41) Cummins, P.; Staples, E.; Penfold, J.; Heenan, R. K. *Langmuir* **1989**, *5*, 1195–1199. 927
- (42) Nakano, M.; Matsuoka, H.; Yamaoka, H.; Poppe, A.; Richter, D. *Macromolecules* **1999**, *32*, 697–706. 929
- (43) Kaewsaiha, P.; Matsumoto, K.; Matsuoka, H. *Langmuir* **2007**, *23*, 9162–9169. 931
- (44) Heerklotz, H.; Tsamaloukas, A.; Kita-Tokarczyk, K.; Strunz, P.; Gutberlet, T. *J. Am. Chem. Soc.* **2004**, *126*, 16544–16552. 934
- (45) He, L.; Garamus, V. M.; Funari, S. S.; Malfois, M.; Willumeit, R.; Niemeyer, B. *J. Phys. Chem. B* **2002**, *106*, 7596–7604. 936
- (46) Edmonds, W. F.; Li, Z.; Hillmyer, M. A.; Lodge, T. P. *Macromolecules* **2006**, *39*, 4526–4530. 938
- (47) Chen, Z.; Cui, H.; Hales, K.; Qi, K.; Wooley, K. L.; Pochan, D. J. *Science* **2004**, *306*, 94–97. 939
- (48) Swanson-Vethamuthu, M.; Feitosa, E.; Brown, W. *Langmuir* **1998**, *14*, 1590–1596. 942
- (49) Zhu, J.; Liao, Y.; Jiang, W. *Langmuir* **2004**, *20*, 3809–3812. 943
- (50) Xuehao, H.; Schmid, F. *Phys. Rev. Lett.* **2008**, *100*, 137802–1 944–4. 945
- (51) Raez, J.; Manners, I.; Winnik, M. A. *J. Am. Chem. Soc.* **2002**, *124*, 10381–10395. 946
- (52) Cornelissen, J. J. L. M.; Fischer, M.; Sommerdijk, N. A. J. M.; Nolte, R. J. M. *Science* **1998**, *280*, 1427–1430. 948
- (53) May, S.; Ben-Shaul, A. *J. Phys. Chem.* **2001**, *105*, 630–640. 949
- (54) Xuehao, H.; Liang, H.; Pan, C. *Phys. Rev. E* **2001**, *63*. 951
- (55) Zehl, T.; Wahab, M.; Mögel, H. J.; Schiller, P. *Langmuir* **2006**, *22*, 2523–2527. 952
- (56) Zehl, T.; Wahab, M.; Schmidt, R.; Schiller, P.; Mögel, H. J. *Mol. Liq.* **2009**, *147*, 178–181. 955
- (57) Nelson, P. H.; Rutledge, G. C.; Hatton, T. A. *J. Chem. Phys.* **1997**, *107*, 10777–10781. 957
- (58) Termonia, Y. *J. Polym. Sci.* **2002**, *40*, 890–895. 958
- (59) Kenward, M.; Whitmore, M. D. *J. Chem. Phys.* **2002**, *116*, 3455–3470. 959
- (60) Marrink, S. J.; Tieleman, D. P.; Mark, A. E. *J. Phys. Chem. B* **2000**, *104*, 12165–12173. 961
- (61) Fujiwara, S.; Itoh, T.; Hashimoto, M.; Horiuchi, R. *J. Phys. Chem. B* **2009**, *130*, 144901. 963
- (62) Pochan, D. J. *Langmuir* **2005**, *21*, 7533–7539. 965
- (63) Uneyama, T. *J. Chem. Phys.* **2007**, *126*, 114902–1–17. 966
- (64) Huang, H.; Chung, B.; Jung, J.; Park, H.-W.; Chang, T. *Angew. Chem., Int. Ed.* **2009**, *48*, 4594. 967
- (65) Larson, R. G. *J. Chem. Phys.* **1985**, *83*, 2411–2420. 969
- (66) Teraoka, I. *Polymer Solutions: An Introduction to Physical Properties*, 1st ed.; John Wiley & Sons, Inc.: New York, 2002. 970
- (67) Mackie, A. D.; Panagiotopoulos, A. Z.; Szleifer, I. *Langmuir* **1997**, *13*, 5022–5031. 972

- 974 (68) Floriano, A. M.; Caponetti, E.; Panagiotopoulos, A. Z. *Langmuir*
975 **1999**, *15*, 3143–3151.
- 976 (69) Ben-Shaul, A.; Gelbart, W. M.; Szleifer, I. *J. Chem. Phys.* **1985**,
977 *83*, 3597–3611.
- 978 (70) Szleifer, I.; Ben-Shaul, A.; Gelbart, W. M. *J. Chem. Phys.* **1985**,
979 *83*, 3612–3620.
- 980 (71) Al-Anber, Z. A.; Bonet-Avalos, J.; Mackie, A. D. *J. Chem. Phys.*
981 **2005**, *122*, 104910.
- 982 (72) Rosenbluth, M. N.; Rosenbluth, A. W. *J. Chem. Phys.* **1955**, *23*,
983 356–359.
- 984 (73) Mackie, A. D.; Onur, K.; Panagiotopoulos, A. Z. *J. Chem. Phys.*
985 **1996**, *104*, 3718–3725.
- 986 (74) Velinova, M.; Sengupta, D.; Tadjer, A. V.; Marrink, S.-J.
987 *Langmuir* **2011**, *27*, 14071–14077.
- 988 (75) Theodorou, D. N.; Suter, U. W. *Macromolecules* **1985**, *18*,
989 1206–1214.
- 990 (76) Gezae, A. Microscopic Modeling of the Self Assembly of
991 Surfactants: Shape Transitions and Critical Micelle Concentrations.
992 Ph.D. thesis, Universitat Rovira i Virgili, 2011.
- 993 (77) Leermakers, F. A. M.; Majhi, P. R.; Dubin, P. L.; Feng, X.; Guo,
994 X.; Tribet, C. *J. Phys. Chem. B* **2004**, *108*, 5980–5988.
- 995 (78) Porte, G.; Appell, J. *J. Phys. Chem.* **1981**, *85*, 2511–2519.